# LANGMUIR

pubs.acs.org/Langmuir Article

# Direct Pore-Level Visualization and Verification of In Situ Oil-in-Water Pickering Emulsification during Polymeric Nanogel Flooding for EOR in a Transparent Three-Dimensional Micromodel

Article Recommendations

Yandong Zhang, Jiaming Geng, Junchen Liu, Baojun Bai, Xiaoming He, Mingzhen Wei,\* and Wen Deng\*



Metrics & More

7.62 mm

2 cm

Glass Beads

ABSTRACT: Different from inorganic nanoparticles, nanosized cross-linked polymeric nanoparticles (nanogels) have been demonstrated to generate more stable Pickering emulsions under harsh conditions for a long term owing to their inherent high hydrophilicity and surface energy. In both core and pore scales, the emulsions are found to be able to form in situ during the nanofluid flooding process for an enhanced oil recovery (EOR) process. Due to the limitation of direct visualization in core scale or deficient pore geometries built by two-dimensional micromodels, the in situ emulsification by nanofluids and emulsion transport are still not being well understood. In this work, we use a three-dimensional transparent porous medium to directly visualize the in situ emulsification during the nanogel flooding process for EOR after water flooding. By synthesizing the nanogel with a fluorescent dye, we find the nanogels adsorbed on the oil—water interface to lower the total interfacial energy and emulsify the large oil droplets into small Pickering oil-in-water emulsions. A potential mechanism for in situ emulsification by nanogels is proposed and discussed. After nanogel flooding, the emulsions trapped in pore throats and those in the effluents are all found encapsulated by the nanogels. After nanogel flooding under different flow rates, the sphericity and diameter changes of remaining oil droplets are quantitatively compared and analyzed using grouped boxplots. It is concluded that in situ emulsification happens during nanogel injection due to the reduction of interfacial tension, which helps to increase the oil recovery rate under different flow rates and pore geometries.

## 1. INTRODUCTION

**ACCESS** 

As fossil energy remains one of the most essential global resources, the demand for oil and natural gas resources is still urgently rising in the next few decades. <sup>1-3</sup> It is well known that about 60–70% of crude oil remains left in subsurface reservoir trapped by capillary force after primary and secondary recovery. <sup>4</sup> Various enhanced oil recovery (EOR) methods, such as thermal, miscible, and chemical methods are applied to extract 30–60% more oil from reservoirs. <sup>5</sup> Nevertheless, new technologies are always desired due to the high demand of energy. Currently, nanoparticles (NPs) have been applied in many areas such as civil engineering, <sup>6</sup> medical applications, <sup>7–10</sup> food science, <sup>11</sup> and solar cells. <sup>12</sup> It also appears to be an alternative for improving different engineering processes in the oil and gas industry, including reservoir characterization, <sup>13</sup> reservoir management, <sup>14</sup> drilling, <sup>15,16</sup> and completion proc-

ess.<sup>17</sup> Besides, the injection of NPs in the form of nanodispersions has also attracted the attention of being used as a potential EOR method due to its small size (1–100 nm) and many other promising interfacial properties.<sup>18–22</sup> Currently, it is widely accepted that the NPs could adsorb onto the interface of two immiscible fluids,<sup>23–25</sup> and this process helps recover more oil by reducing interfacial tension (IFT),<sup>21,24,26,27</sup> altering wettability,<sup>28–30</sup> modifying disjoining pressure,<sup>31,32</sup> and stabilizing Pickering emulsions.<sup>33–35</sup> How-

Supporting Information

Received: July 30, 2021
Revised: October 13, 2021
Published: November 1, 2021





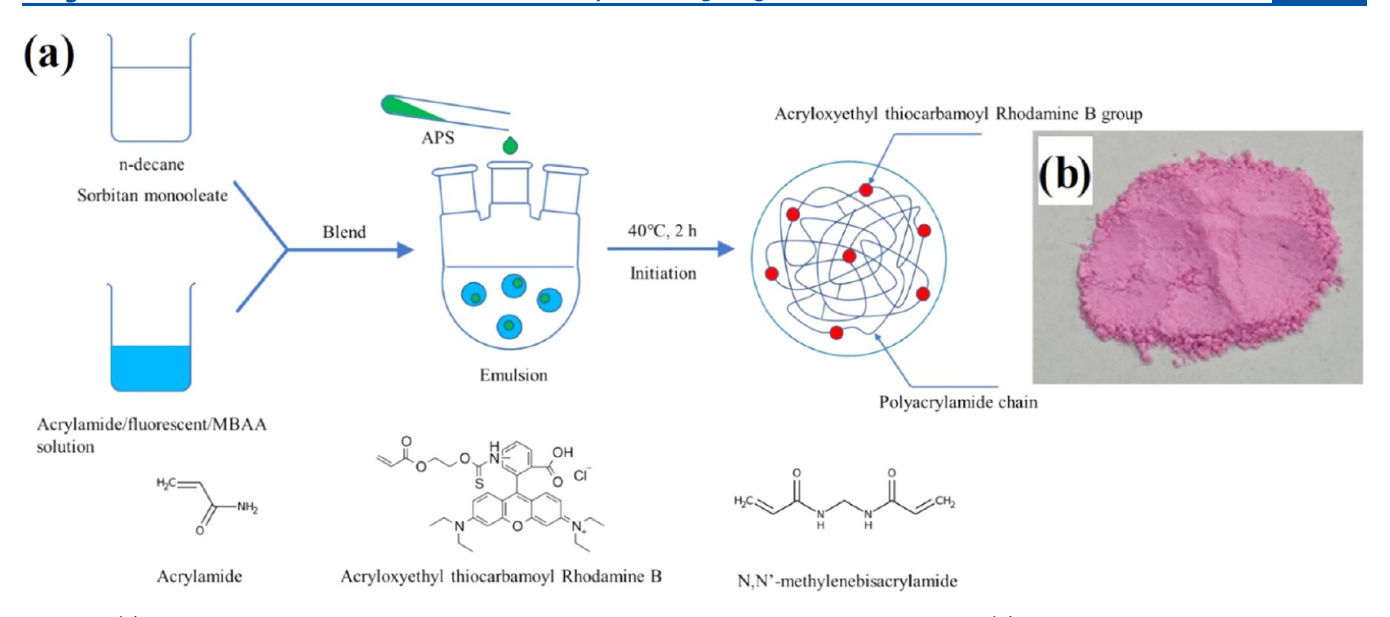


Figure 1. (a) Schematic diagram of the synthesis of the fluorescent-dyed cross-linked polymeric nanogel; (b) sample of the dry fluorescent nanogel powder.

ever, the mechanisms of NPs for extra oil recovery are still not well understood so that field applications are not widely applied and relevant research mostly is based on laboratory core flooding experiments.<sup>36–39</sup>

Among the suggested mechanisms of NPs for EOR, the oilin-water Pickering emulsion generation and stabilization by NPs have been increasingly studied in recent years due to its better resistance under harsh conditions than surfactants and can be injected for improved mobility control under highsalinity condition. 33,40 However, most of the currently used NPs are inorganic NPs and can be tailor-made for specific surface modifications with grafted polymer chains, without which the stable Pickering emulsion with high resistance to harsh conditions cannot be formed. 3,41-44 These modifications significantly raised the budget and increased the production time. Except for polymer-grafted NPs, another choice is the hybrid polymer nanofluid suspension by directly mixing or blending nanoparticles into the polymer. Although it was reported to be easily synthesized, it is hard to obtain a uniform dispersion due to the strong tendency of nanoparticle aggregation in the polymer matrix.45

Compared to the Pickering emulsion stabilized by rigid NPs, the soft nanogel stabilized Pickering emulsions have attracted much attention due to their temperature and pH-responsive properties.<sup>46</sup> When adsorbing onto oil-water interface, their inherent high hydrophilicity and sufficient steric repulsion can prevent coalescence of oil droplets, which enables the longterm stabilization of Pickering emulsions, even at high temperatures. 47,48 Other than injecting prepared micro/ nanoemulsions or NP-stabilized surfactant or foam injections for EOR, 49 it was also observed that the solely nanogel dispersion injection after water flooding in sandstone could generate in situ shear-induced oil-in-water emulsion as the produced effluent after water flooding was in bulk oil phase while in oil-in-water emulsion state after nanogel flooding. The adsorbed nanogel layer ensures that the emulsified oil droplets are stable and isolated before being produced to the surface.<sup>50</sup>

Due to the difficulty of direct visualization of the fluid flow process within a core, the in situ emulsification phenomenon during nanogel flooding cannot be easily visualized.<sup>51</sup> There-

fore, microfluidic models become a powerful tool to investigate the microscopic mechanisms of NPs for EOR, including the in situ emulsification.<sup>52</sup> Since most available microfluidic studies were based on a two-dimensional (2D) micromodel, it is inherently difficult to study emulsion or foam flow due to the limited pore geometry, 53,54 most of which focused only on the investigations of IFT reduction and wettability alteration caused by NPs<sup>55-58</sup> while a few discussed the NP-stabilized emulsion flow using an emulsion generator or the so-called "2.5D micromodel" in the literature. $^{58-61}$  The most recent three-dimensional (3D) transparent micromodel packed with glass beads was only used to directly visualize the two-phase fluids flow behaviors and a core-shell nanohydrogel for conformance control under a confocal microscope. 62-65 To the best of our knowledge, no research has been done to directly visualize the in situ emulsification during the nanogel flooding using a 3D micromodel, which is a more proper candidate to study the emulsification mechanism with more realistic discontinuous pore throats and pore bodies.

Therefore, in this work, we aim to investigate the in situ emulsification of remaining oil induced by solely fluorescent polymeric nanogel flooding for EOR using a 3D transparent micromodel with microheterogeneities. How the in situ emulsions are generated during the nanogel flooding and how the change of remaining oil shape and size before and after nanogel flooding are visualized and studied. The main contents can be given as below. We first introduce the synthesis of the fluorescent nanogels and describe the properties of the prepared fluids. Then, we present the micromodel characteristics and our detailed experimental procedures. Following are the results and discussions to demonstrate our findings. Quantitative analyses are given to clarify the in situ emulsification phenomenon during the nanogel flooding.

#### 2. EXPERIMENTAL SECTION

**2.1. Materials.** Acrylamide was purchased from Xinwantong Company (Daqing, China), acryloxyethyl thiocarbamoyl Rhodamine B (95–100%) was from Polysciences, Inc. N,N'-methylenebisacrylamide (MBAA, 99%) from Sigma-Aldrich, ammonium persulfate

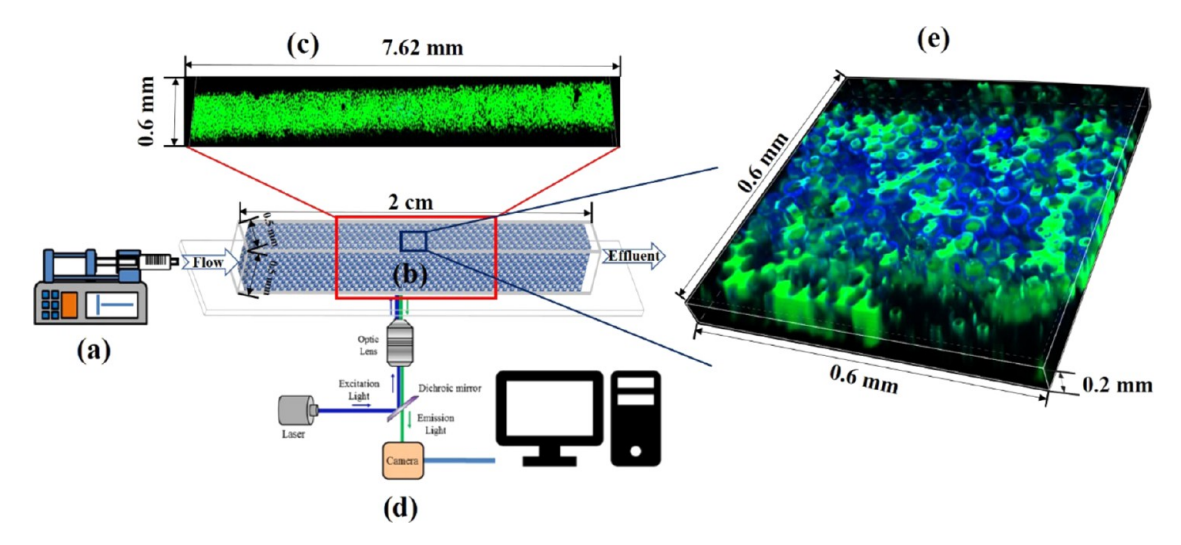


Figure 2. Schematic of the experimental setup. (a) Syringe pump for injection of fluids. (b) Transparent porous medium built by packed glass beads. (c) Example of static global visualization of an oil-saturated model. (d) Confocal laser scanning microscope system for visualizing the fluid flow process inside the model. (e) Example of the dynamic local visualization of a 3D acquisition during the water flooding (oil in green and water in blue).

(98%) from Acros Organics, and N-decane (99%) from Alfa Aesar were used in our experiments. Deionized water was prepared in the laboratory using an ultrapure water system. Sorbitan monooleate was purchased from Alfa Aesar. Poly(ethylene glycol) sorbitan monostearate was purchased from Sigma-Aldrich.

**2.2.** Synthesis of Fluorescent Polyacrylamide Nanogels. Fluorescent polyacrylamide nanogels are synthesized using a reverse suspension polymerization. The synthesis process is shown in Figure 1a. For a typical experiment, 15 g of acrylamide, 20 mg of acryloxyethyl thiocarbamoyl Rhodamine B, and 2.25 mg of MBAA are dissolved in 15 g of deionized water. Then, the aqueous solution is added into the mixture of 7 g of Span 80, 3 g of Tween 60, and 40 g of decane. After purging nitrogen for 15 min, 2 mL of 2% APS aqueous solution is added to initiate the polymerization. The reaction is kept at 40 °C for 2 h to form nanogels. Afterward, the nanogels are precipitated in acetone and washed with acetone three times using centrifugation. The nanogel is then collected and dried before adding to any fluids, as shown in Figure 1b.

2.3. Micromodel Characteristics and Fluid Preparation. We fabricate the 3D transparent porous media by lightly sintering the borosilicate glass beads (Mo-Sci) densely packed in a squared quartz capillary tube (L: 2 cm; W: 0.5 mm; H: 0.5 mm; T: 0.25 mm; Technical Glass Products, Inc.) under 850 °C for 100 s. The capillary tube is packed with two sizes of glass beads (small-to-big-number ratio of 3:1) with the radii of r = 17 and 65  $\mu$ m. The pore diameters are estimated between 5 and 21  $\mu$ m.<sup>69</sup> Due to the random packing, the pore geometries are different for eight models and the average porosity is 42%. The porosity is determined after oil saturation process and would be discussed in the following section. The permeability can thus be estimated as 4.1  $\mu$ m<sup>2</sup> using the Kozeny-Carman relation,  $k = a^2 \varphi^3 / 45(1 - \varphi)^2$ , where *a* is the average sphere radius and  $\phi$  is the average porosity. To overcome the limitations that scattering lights from interfaces of fluid/fluid and fluid/solid would preclude the direct observation of the multiphase flow within the 3D porous media, an immersion aqueous liquid (Cargille Labs;  $\rho$  = 1.921 g/cc;  $\mu = 7.684$  cP) and immersion oil (Cargille Labs;  $\rho = 0.855$  g/cc;  $\mu$  = 18.81 cP) are used as the wetting phase and the nonwetting phase to keep the refractive index the same as the quartz capillary tube and glass beads with RI = 1.47. The interfacial tension between two fluids is  $\sigma \approx 12$  mN/m measured using the pendant drop method (see Figure S1 in the Supporting Information). The nanofluid is then prepared by adding 0.2 g of fluorescent polyacrylamide nanogels into 100 mL of immersion aqueous liquid where the concentration of nanogels is controlled as low as 0.1 wt %, which would not significantly increase the wetting phase viscosity. 70 To ensure the

nanogels in almost fully swollen state, the prepared nanofluid is stirred for 1 h and then stored at 65 °C for 24 h before any characterization and experiments (see Figure S2 in the Supporting Information). To distinguish the two kinds of fluids and nanogels under different lasers, they are all fluorescent dyed differently: AlexaFluor 647 for the water phase, Nile Red for the oil phase (Sigma-Aldrich), and methacryloxyethyl thiocarbamoyl rhodamine B (Polysciences) for nanogels, respectively. The water phase is in blue, the oil is in green, and the nanogels are in red after separately excited by lasers at 647, 488, and 561 nm.

2.4. Experimental Setup and Procedure. To visualize the dynamic fluid flow inside the micromodel, we mount each micromodel on a Nikon A1R HD inverted confocal laser scanning microscope (Eclipse Ti2) as shown in Figure 2 for the schematic of the experimental setup. A syringe pump (Harvard Apparatus PHD ULTRATM) is used to inject the fluids at the inlet of the model through a fused silica capillary tubing with a 100  $\mu$ m inner diameter, and the effluent is collected at the outlet. We use two modes of visualization for each experiment: one is the static global mode and the other is the dynamic local mode. The static global mode is used after oil saturation, water flooding, and nanogel flooding to reveal the final fluid phase distribution at each end of the flooding process. We use a 20× objective lens to scan the middle regions of the model to avoid the tubing influences at the inlet and the outlet where the beads are not being compactly packed. The stage is set moved automatically from left corner inlet to right corner outlet with 13 horizontal steps (7.62 mm) along the x direction, 2 vertical steps (0.6 mm) along the y direction, and 200  $\mu$ m in depth along the z direction constructed from 40 optical slices spaced by 5  $\mu$ m. All fields are then stitched together (5% overlap) to obtain a complete 3D image of the model. The dynamic local mode is used to study the zoom-in displacement process within the porous media in which the region of interest is chosen as the middle part. We scan and record the whole injecting process during water and nanogel flooding using resonant scanning mirrors instead of traditional galvanometer mirrors to acquire a high scanning speed. Each 3D acquisition is constructed with 20 optical slices in a 0.6 mm  $\times$  0.6 mm x-y plane and spaced by 10  $\mu$ m along the z direction with 200  $\mu m$  in depth along the z direction. Although the resolution becomes worse when using a resonant scanner, the fast acquisition time for an entire 3D acquisition is approximately 14 s, which enables the visualization of the fluid flow details. All experiments are conducted at room temperature.

**2.5. Oil Saturation Process.** In this research, since our focus is to observe the effect of fluorescent nanogels on emulsifying the remaining oil droplets after water flooding, we do not consider the

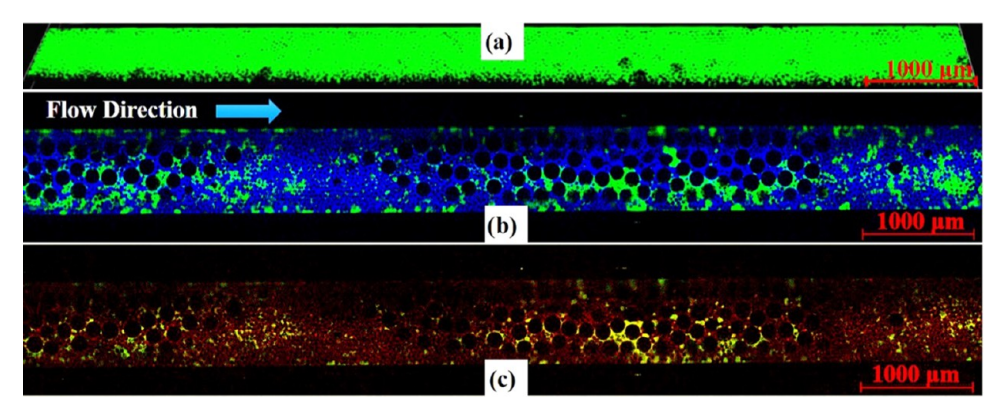


Figure 3. Static global visualization examples after (a) oil saturation, (b) water flooding process, and (c) nanogel flooding process (oil in green, water in blue, and nanofluid in red).

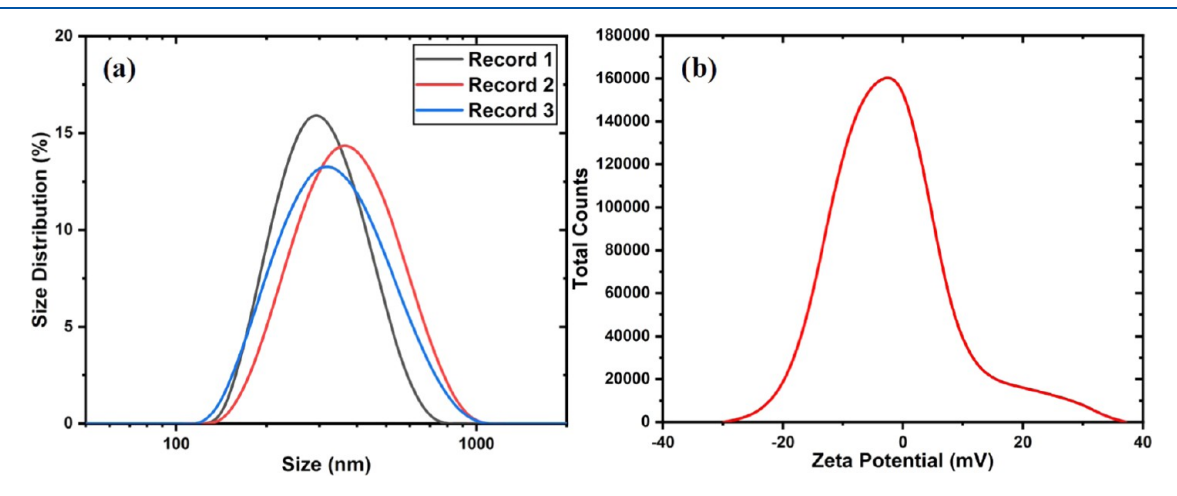


Figure 4. Characteristics of fluorescent dyed nanogel. (a) Particle size distribution based on the DLS method and (b)  $\zeta$  potential distribution.

irreducible water saturation to mimic the real reservoir saturation history. Therefore, we directly saturate the model with oil first and then conduct water flooding and nanogel flooding. The micromodel is first saturated with the immersion oil injected using a syringe pump (Harvard Apparatus, model 88-3015) for 24 h at a flow rate of 0.005 mL/h through a fused silica capillary tubing with a 100  $\mu$ m inner diameter. The flow direction is from left inlet to right outlet, which is always open to the air with no backpressure added. As shown in Figure 3a, the 3D porous medium is fully saturated with the green oil phase. Since the oil occupies all of the pore volume, we then use the saturated oil volume to determine the effective porosity as  $\emptyset = V_V/V_T$ =  $V_{o}/V_{T}$ , where  $V_{V}$  is the volume of pore spaces,  $V_{o}$  is the volume of the saturated oil in pore spaces, and  $V_{\mathrm{T}}$  is the total volume, which includes the pore spaces and the glass beads. The total volume is  $5.115 \times 10^8 \,\mu\text{m}^3$ , calculated by multiplying the visualized area and the height. We only chose the middle part of the model to visualize. However, the outlet region with tubing inserted can be used to verify the assumption for the interface conditions governing the coupled flow in a porous medium and its adjacent conduits. The two different sized glass beads and the void spaces between the tubing and the tube wall can be regarded as the porous medium and conduits, respectively.7

**2.6. Water and Nanogel Flooding Process.** We conduct forced water imbibition processes after oil saturation with different constant flow rates of 0.002, 0.02, 0.04, 0.06, 0.08, 0.1, 0.8, and 20 mL/h, spanning the capillary number from  $10^{-6}$  to  $10^{-2}$ , which is defined as  $Ca = \mu_{\rm nw}Q_{\rm inj}/A\sigma$  (where  $\mu_{\rm nw}$  is the injection fluid viscosity,  $Q_{\rm inj}$  is the injection rate, A is the cross-sectional area of the micromodel, and  $\sigma$  is the interfacial tension between the wetting and nonwetting fluids). To better show the flooding performances, we here choose one representative 2D layer of water flooding under 0.8 mL/h as an

example shown in Figure 3b. The oil phase and water phase are in green and blue, respectively. All flooding processes are stopped after 10 PV (pore volume) of injection when no more significant phase changes within the micromodels. Later, nanogel flooding is also conducted using the same flow rates and PVs. As shown in Figure 3c, the nanogel suspension fluid is in red with dispersed fluorescent dyed nanogels. After finishing all of the experiments, we use NIS Elements software to binarize, segment the water, oil, and nanogel fluid, and perform a quantitative analysis. Detailed results and discussions are presented in the next section.

### 3. RESULTS AND DISCUSSION

3.1. Size and  $\zeta$  Potential of the Nanogels. The size distribution and  $\zeta$  potential of the synthesized nanogels are measured using a Malvern ZS90 Nanosizer at a scattering angle of 90° with an incident beam of a wavelength at 633 nm at 30 °C (see Figures S3 and S4 in the Supporting Information for size distribution and  $\zeta$  potential under different temperatures). The prepared 500 ppm nanofluid is directly injected into the glass cuvette and folded capillary  $\zeta$  cell for size and  $\zeta$  potential measurements, respectively. The intensity size distribution is obtained from analysis of the correlation functions using the multiple narrow mode algorithms in the Instrument software, which is repeated three times for the same sample fluid. The final size distribution of the nanogel dispersion fluid is shown in Figure 4a, where the distribution range is from 150 to 1000 nm and the peak of the nanogel distribution falls between 250 and 300 nm. For the  $\zeta$  potential shown in Figure 4b, it appears in the range of around -1 to -5 mV, which can be regarded as

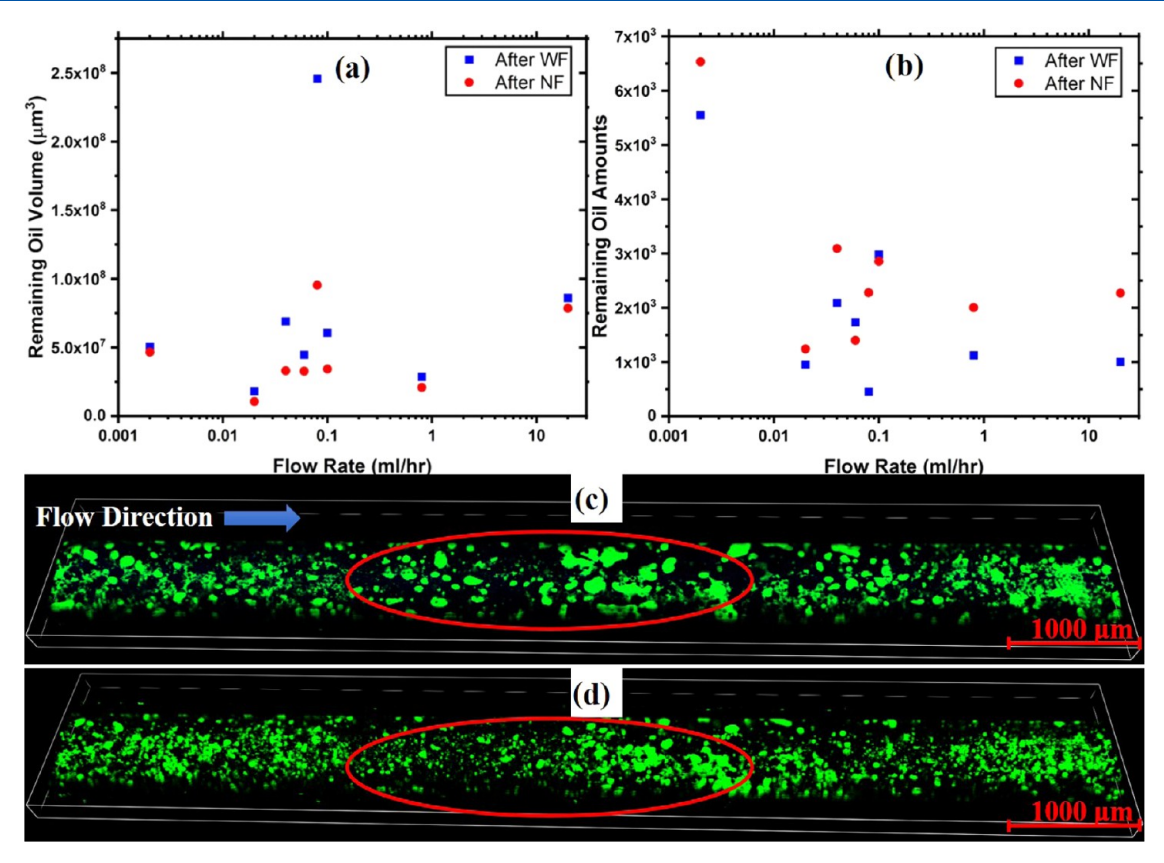


Figure 5. (a) Remaining oil volume and (b) remaining oil amounts under different flow rates after water and nanogel flooding. Remaining oil distribution after (c) water flooding and (d) nanogel flooding under a flow rate of 0.8 mL/h (oil in green).

neutral charged nanogels. It has been studied that neutral charged nanogels exhibit the highest and longest performance on stabilizing the oil-in-water Pickering emulsions. <sup>47</sup> Even though the absolute value of  $\zeta$  potential is very low, this cross-linked high molecular nanogel could still be stable by providing steric hindrance. <sup>66</sup> Besides, the lightly negative surface charge could minimize the adsorption of the nanogels onto the glass beads, which acquire also a negative surface charge in water, <sup>67</sup> to reduce the factor that may affect the emulsification process. <sup>68</sup>

**3.2.** In Situ Emulsification. The in situ emulsification process and results are observed during and after nanogel flooding using two modes of visualization. We find that for all experiments under different flow rates, the number of remaining oil droplets increases after nanogel flooding while the total remaining oil volume decreases. As shown in Figure 5a, it does not show a clear relationship between different flow rates and remaining oil droplets volume due to the random packed porous geometries of different micromodels. However, it does show that the remaining oil droplet volumes after nanogel flooding are less than those of after water flooding under each flow rate. For the remaining oil droplet amounts as shown in Figure 5b, it shows a decrease from the lowest to the highest flow rate for both after water and nanogel flooding. Besides, the number of remaining oil droplets after nanogel flooding is always more than that after water flooding for all cases. Figure 5c,d shows the representative cases of the final remaining oil droplets distribution after water flooding and nanogel flooding under a flow rate of 0.8 mL/h. We only include the green color for oil to eliminate other interference. It is evident that the bigger remaining oil droplets after water

flooding turn to be smaller oil droplets after nanogel flooding as demonstrated in the red circle in Figure 5c,d.

An in situ emulsification process in a local region under the flow rate of 20 mL/h is shown in Figure 6a-f, since the highest flow rate could emulsify more oil clusters than other lower flow rates from Figure 5b. At T = 0 s, the remaining oil after water flooding is distributed as connected large clusters and the nanogel fluid is about to enter this region. At T = 14 s, most of the bulk remaining oil is emulsified and displaced, while there are still some oil droplets trapped in the pores. From T = 14 to T = 70 s, we observe that the emulsified oil droplets are still being displaced within the pore throats, but some emulsions are left and trapped in the end, which cannot be recovered. Especially for the middle group of oil droplets, which are easily displaced through the pore space between two bigger glass beads from T = 14 to T = 42 s in Figure 6b-d, they begin to snap off when they go through the thinner pore throats consisting of smaller glass beads from T = 42 to T = 70 s in Figure 6d-f. Finally, at T = 70 s, there are no more emulsions moving in the whole region and some emulsions that cannot be displaced under the current scenario are trapped as residual oil-in-water emulsion droplets. We collect a small amount of effluent after nanogel flooding and visualized within a local region. The 2D view in Figure 6g (left) shows all of the emulsions are in perfect round shapes and the sizes of the emulsions are mostly from about 2 to 20  $\mu$ m in diameter. However, we find that the minimum trapped oil droplet diameter is around 6  $\mu$ m, which is close to the minimum pore size of 5  $\mu$ m. It indicates that the emulsified oil droplets smaller than pore throat are displaced out of the model completely as the continuous phase. From the 3D view in Figure 6h (right),

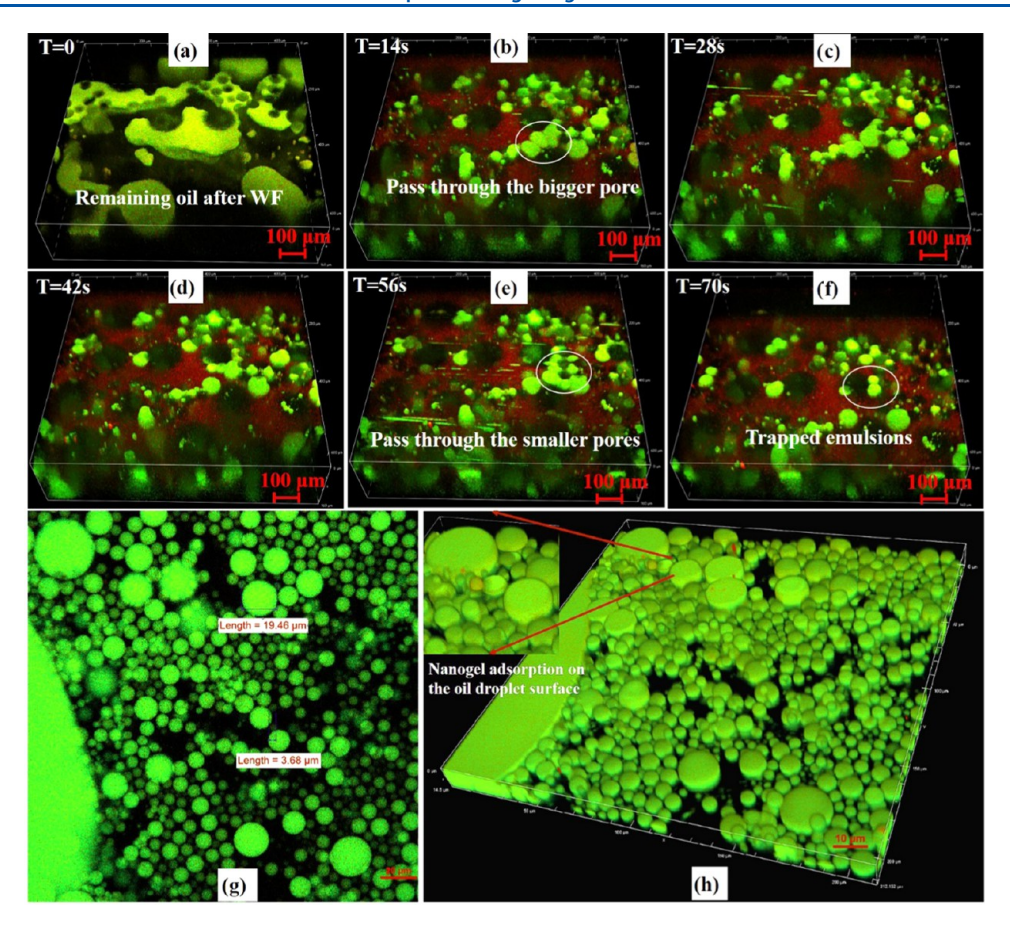


Figure 6. (a-f) In situ emulsification process example in a local region under the flow rate of 20 mL/h, and the emulsion droplets in the effluents in (g) 2D and (h) 3D views, showing the diameters of the displaced emulsions of around 2–20  $\mu$ m and the adsorbed red nanogels on the interface (oil in green and nanogel/fluid in red).

it is clear that the red nanogels are absorbed on the droplet sphere surface, although the sizes are small and the signal intensity is not as strong as the microgels, which are easier to be detected.<sup>74</sup> The video in the Supporting Information (SI) shows the local water flooding process and the nanogel flooding process, where one could observe the clear emulsification process during the nanogel flooding to displace more remaining oil droplets out of the porous medium.

However, not all remaining trapped oil droplets after water flooding can be emulsified and displaced during the nanogel flooding process, although it was believed that snap-off would happen at higher capillary numbers if the pore size is much smaller than the droplet size.<sup>75</sup> Figure 7a-f displays an unsuccessful emulsification process for a trapped remaining oil droplet after water flooding under the capillary number of  $10^{-2}$ . At T = 0 s, the original droplet is trapped in the pore space between the glass beads. From T = 16 s, we observe that the red nanogels adsorb onto the front meniscus of the droplet and start to emulsify and drag the droplet. The droplet deformation reaches the maximum at T = 57 s but back to the original shape at T = 71 s. Then, the second emulsification attempt occurs at T = 114 s when the droplet is once again dragged into the pore throat. Finally, as the droplet fails to be emulsified, it changes back to the original shape for the second time at T = 268 s and no further deformation is observed. The final shape of the droplet is shown to have a larger surface area than the initial form, which indicates a sphericity decrease. Besides, more nanogels are shown adsorbed on the front

meniscus, which indicates that the nanogels could be trapped together with the droplet at the entrance of the pore throat and keeps it as stabilized oil-in-water emulsion droplet. This finding is consistent with the Lattice Boltzmann simulation result, which shows that the viscous shear force is supplied by the outer fluid (nanofluid in our experiments) against the interfacial tension when flows pass the oil droplet that causes the droplet snap-off near the pore throat exit. The unsuccessful emulsification would lead to the capillary trapping of the residual oil droplets shown in Figure 7g, which are also regarded as the trapped oil-in-water emulsion droplets. The trapped emulsion droplet may play a role as an in-depth diversion agent for conformance control.<sup>77</sup> As shown in Figure 3b, the low-permeability regions of small glass beads are barely swept, but it turns red after nanogel flooding in Figure 3c, indicating that bigger pores consisting of bigger glass beads have been clogged by the trapped oil-in-water emulsions. As we expect, the residual oil droplets are in low sphericity and the nanogels are mostly found on the front meniscus of the droplets with the flow direction from left to right.

**3.3. Remaining Oil Droplets Characterizations.** Sphericity of an oil droplet, defined as  $\psi = (6\pi^{1/2}V_p)^{2/3}/A_p$  (where  $V_p$  and  $A_p$  are the droplet volume and surface area, respectively), is a measure of how spherical an oil droplet is. By definition, the more the shape of an oil droplet is close to a sphere, the more spherical it is as the sphericity is closer to  $\psi = 1$ . Oppositely, nonspherical oil droplets always have sphericity less than  $\psi = 1$  and close to  $\psi = 0$  when they are having larger

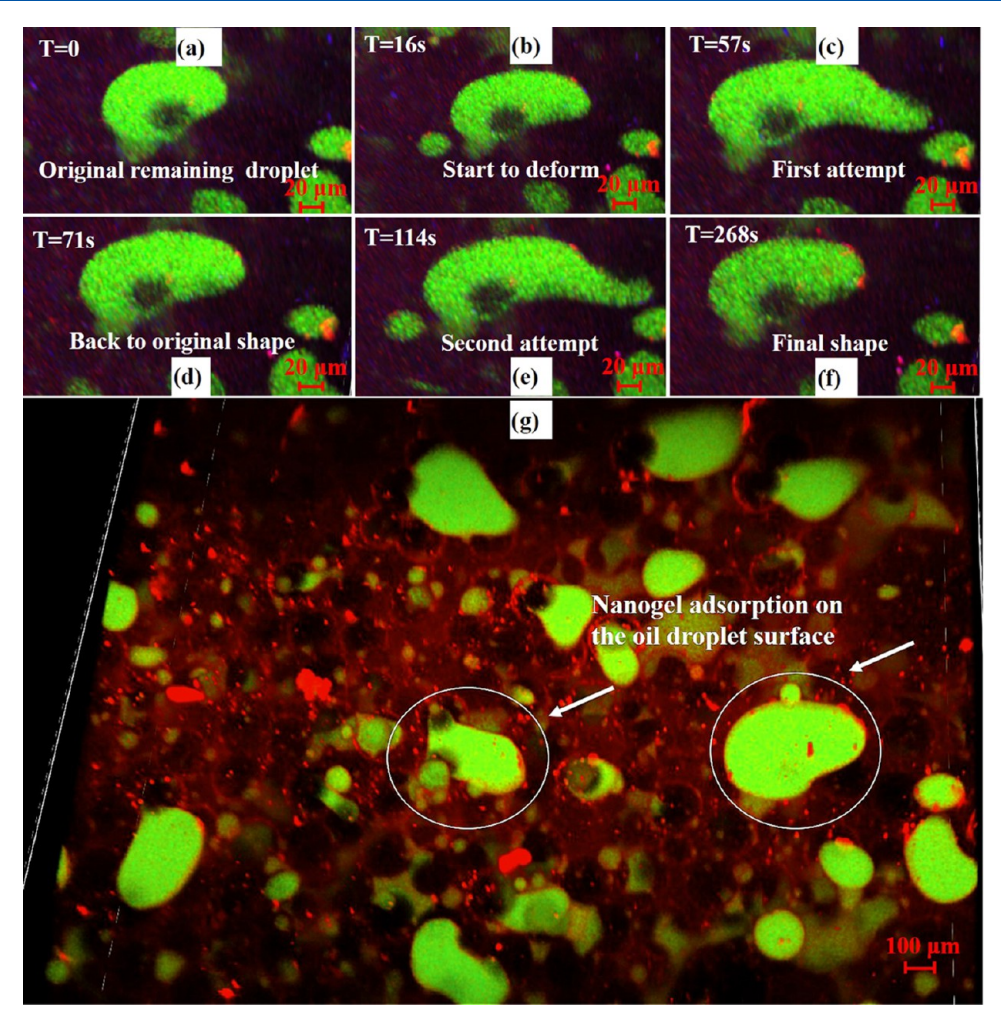


Figure 7. (a-f) Unsuccessful in situ emulsification process example for a large trapped oil droplet in a local region under the flow rate of 20 mL/h. (g) Trapped emulsions in the porous medium were encapsulated by the adsorbed red nanogels mostly on droplet front meniscus (oil in green and nanogel/fluid in red).

volumes and surface areas that the shapes are far from spherical. To compare the sphericity after water flooding and nanogel flooding under different capillary numbers, we plot the grouped boxplot to give an intuitive comparison as shown in Figure 8a. Interestingly, we find the mean sphericity of the remaining oil droplets after nanogel flooding decreases by comparing to that after water flooding in five out of eight experiments, which are conducted under lower capillary numbers. However, the sphericity of remaining oil droplets after nanogel flooding increases by comparing to that after water flooding for two experiments under higher capillary numbers. For the smallest capillary number, the sphericity does not show much change but a slight increase. The reason to cause the remaining oil droplet sphericity difference after water and nanogel flooding can be attributed to the oil/water interfacial tension reduced by nanogel adsorption.<sup>78</sup> The adsorption on the oil/water interface may also change the oil droplet surface wettability, which would lead to the sphericity reduction of the trapped remaining oil droplets after water flooding. We therefore raise a discussion for how this wettability change induces sphericity reduction in the porous media based on our direct observation using a confocal microscope.

The suggested sphericity-changing process for a trapped remaining oil droplet by nanogel adsorption is shown in Figure

9c. Originally, a hydrophobic remaining oil droplet is trapped in pore throat due to the capillary pressure after water flooding. The hydrophilicity of the glass bead results in a large (over 100 degree) contact angle between the oil droplet and the glass bead so that the trapped oil droplet remains highly spherical in shape with the sphericity close to  $\psi = 1$ . As the later introduced nanogel fluid flows toward the oil droplet, they immediately adsorb onto the oil/water interface and encapsulate the whole droplet, which is very similar to the recently reported Janus amphiphilic nanosheets climbing onto the oil-water interface. An example of oil droplet sphericity change after water and nanogel flooding is shown in Figure 9a,b. It is evident that the sphericity decreases after the nanogel flooding as the droplets become nonspherical (droplets are highlighted for better segmentation). Even though we are unable to capture this adsorption process due to the limitation of the frame rate, we find that the trapped oil droplets after nanogel flooding are all encapsulated completely by red nanogels as shown in Figure 7g, and so do the displaced emulsion droplets as shown in Figure 6g,h. Therefore, it indicates that the nanogels can climb into the gap between the oil droplet and the glass bead to form a thin nanogel layer. Since the glass bead and the nanogel are both hydrophilic, the contact angle between the oil droplet with adsorbed nanogels and the glass beads becomes smaller as the nanogel thin layer tends to spread along the glass bead. As

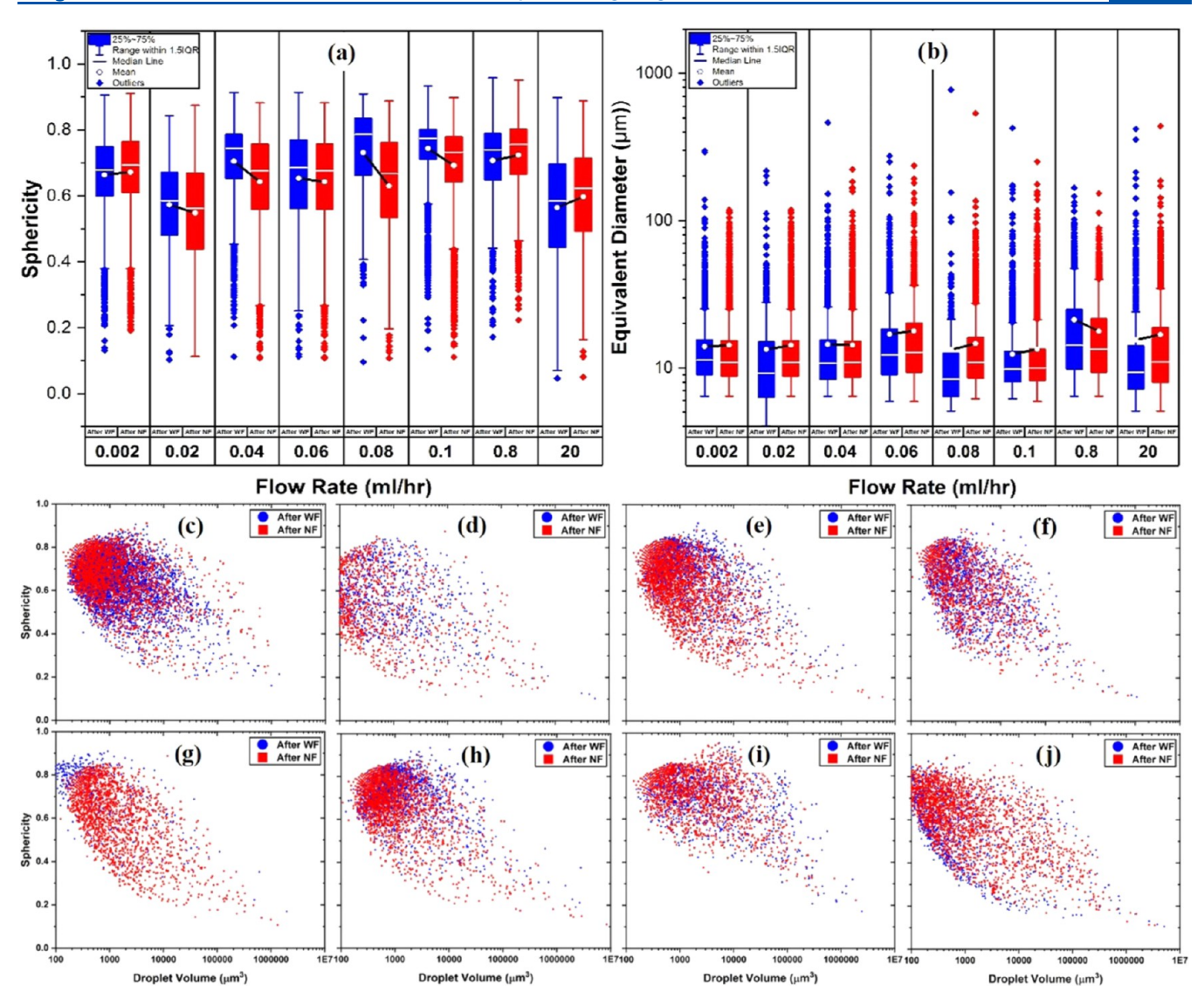


Figure 8. Grouped boxplots of (a) remaining oil droplets sphericities and (b) equivalent diameters after water and nanogel flooding under different flow rates. (c-j) Relationship between the remaining oil droplets sphericity and the volume after water and nanogel flooding under different flow rates from 0.002 to 20 mL/h.

a result, the shape of the oil droplet becomes less spherical due to the nanogel adsorption. Meanwhile, part of the oil droplet was emulsified by the passing flow into micro-sized oil-in-water emulsions that cannot be trapped. If the emulsion droplet size is very small compared with the pore and throat diameters of a porous medium, the emulsion can be regarded as a continuous phase. As shown in Figure 9a, the remaining oil droplets exhibited high sphericity after water flooding while the sphericity decreases a lot after nanogel flooding, as shown in Figure 9b, where the shapes become more irregular, meanwhile indicating the decrease of interfacial tension due to the nanogel adsorption.

However, the sphericity of oil droplets after nanogel flooding increases when the flow rate becomes higher. As shown from the grouped boxplots in Figure 8a, when the flow rates are 0.8 and 20 mL/h, the sphericity of oil droplets after nanogel flooding increases. It indicates that the higher flow rate could induce a higher shear rate, under which the bigger residual oil droplets at the model boundary could be emulsified into more small oil droplets. The total volume and the surface area of the residual oil droplets both decrease a lot, hence the sphericity

increases thereafter. At lower flow rates, the bigger residual oil droplets stuck to the boundary are not likely to be emulsified and displaced; thus, the sphericity is still decreased even though the residual oil droplets in porous media decrease since the total volume does not have a significant decrease, but the surface area increases. The equivalent diameters of the remaining droplets under different flow rates were also displayed in a grouped boxplot as shown in Figure 8b. At lower flow rates, the diameter of the oil droplets does not change very much as the driving force is not large enough to move a large amount of oil. However, as the flow rates became higher, the oil droplet diameters increased as the pressure gradient became higher to emulsify more remaining oil, which caused some bigger emulsion droplets trapped in the porous media. It showed that the emulsion flow during nanogel flooding was not sensitive but became unstable at higher flow rates,<sup>75</sup> which is also consistent with a recent study of porescale emulsion flow in porous media.80

Figure 8c-j displays the relationship between the volume of remaining oil droplets and the sphericity after water and nanogel flooding under different flow rates. This figure first

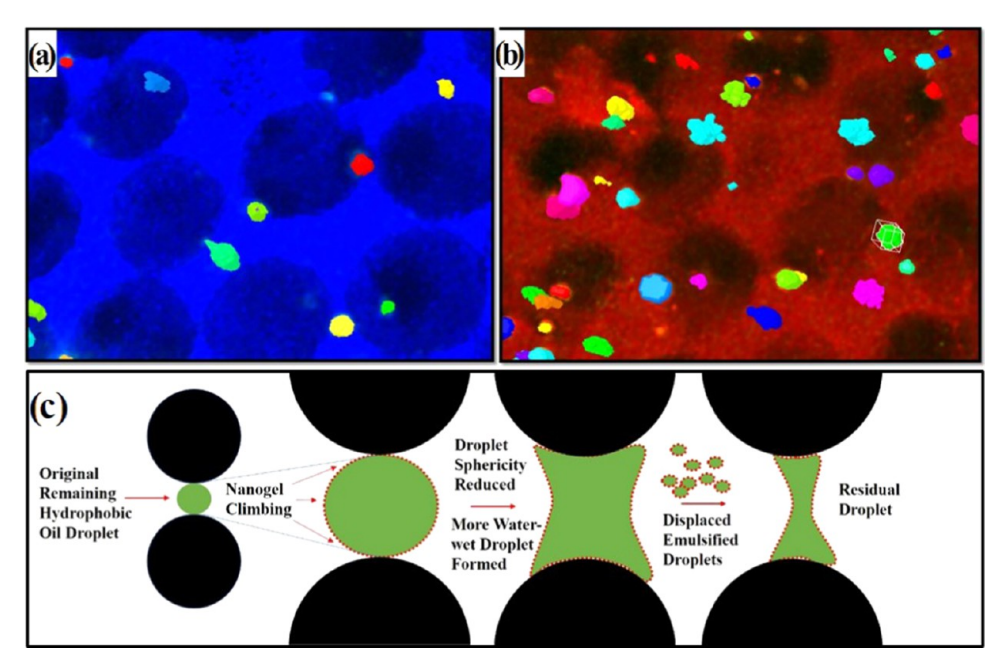


Figure 9. Remaining oil droplets sphericity after (a) water and (b) nanogel flooding (all droplets were highlighted in colors for better segmentation). (c) Suggested mechanism of the emulsification process of remaining oil droplets by nanogel in a pore throat.

Table 1. Enhanced Oil Recovery under Different Flow Rates

model no.	porosity %	flow rate (mL $h^{-1}$ )	capillary number	oil recovery (WF)/%	oil recovery (NF)/%	oil recovery (total)/%
1	46	0.002	$1.4 \times 10^{-6}$	78.1	1.7	79.7
2	41	0.02	$1.4 \times 10^{-5}$	88.2	5.0	93.1
3	40	0.04	$2.8 \times 10^{-5}$	76.1	12.5	88.6
4	40	0.06	$4.3 \times 10^{-5}$	46.8	14.1	60.9
5	44	0.08	$5.7 \times 10^{-5}$	34.4	40.2	74.5
6	37	0.1	$7.1 \times 10^{-5}$	82.7	7.6	90.2
7	38	0.8	$5.7 \times 10^{-3}$	89.6	2.8	92.4
8	42	20	$1.4 \times 10^{-2}$	82.4	1.5	83.9

gives an intuitive visualization that the remaining oil droplets after nanogel flooding (the red dots) are more than remaining oil droplets after water flooding (the blue dots). Besides, we find that the sphericity of a trapped oil droplet decreases as its volume increases under each flow rate, indicating that a larger oil droplet has a relatively larger surface area compared to its volume. For an oil droplet with volume larger than 0.001 mm<sup>3</sup>, the sphericity is smaller than  $\psi$  < 0.2. This kind of larger remaining oil cluster is often found stuck to the tube walls, which are less water-wet and in flat sheetlike shape far from spherical, which could hardly be emulsified and displaced at low flow rates and almost remained the same volume after nanogel flooding. We find that most of the remaining oil droplets after water flooding have low sphericity even though the volume is small under a high flow rate of 20 mL/h in Figure 8j, which indicates that they are unswept and trapped due to the viscous fingering. However, the mean sphericity increases after nanogel flooding, and it can be found in Figure 8j that the oil clusters with low sphericity have been swept and emulsified into small oil droplets with higher sphericity. This observation indicates that the nanogel flooding at high flow rates, other than low flow rates, is more likely to improve the microheterogeneities of the porous media and emulsify large oil clusters into small oil droplets, resulting in an increase of mean sphericity due to the decrease in the total volume and surface area.

**3.4. Enhanced Oil Recovery.** The oil recovery after water flooding and nanogel flooding and the total oil recovery under different flow rates are shown in Table 1.

We find that the oil recoveries after water flooding are not monotonically increased with the increase of capillary number or model porosities. This experimental observation is due to the disordered packing of the glass beads, 81 which is different from the previous experimental results of homogeneous porous media packed by single-sized glass beads. 64 Besides, the increased oil recoveries after nanogel flooding are higher when the oil recoveries after water flooding are low. On the contrary, when oil recoveries after water flooding are high, the oil recoveries after nanogel flooding are relatively low. As shown in Table 1, the experiment under a flow rate of 0.08 mL/h only achieves 34.4% oil recovery after water flooding, which can be regarded as a special case due to the loose packing of the micromodel. However, the total oil recovery increases to 74.5% after nanogel flooding, which is a 40.2% increase compared to water flooding. When the oil recovery after water flooding is 89.6% under the flow rate of 0.8 mL/h, the extra oil recovery by nanogel flooding is only 2.8%. Therefore, the remaining oil saturation after water flooding may affect the nanogel flooding performance. When the remaining oil saturation is high, most of the trapped oil in the unswept zone is maintained in the form of connected bulk phase. When there are less remaining trapped oil droplets dispersed in separated pores, it becomes

much harder for the nanogels to emulsify and recover due to the increased capillary force even though the nanogels could still help recover a small amount of remaining oil droplets by reducing the interfacial tension and emulsification. All in all, regardless of the condition of pore geometries, flow rates, or water flooding performances, the nanogel demonstrates its ability to improve oil recovery after water flooding.

#### 4. CONCLUSIONS

To conclude, we successfully synthesize the polymeric nanoparticles with a fluorescent dye and directly visualize their roles on emulsifying the remaining oil droplets during the nanogel flooding under different flow rates within a 3D transparent micromodel using a confocal microscope. Under the dynamic local visualization mode, we capture the in situ emulsification processes with two scenarios. For the successful emulsification scenario, we find that the bulk form of remaining oil clusters after water flooding is emulsified by nanogels into small oil droplets and some of these emulsion droplets are trapped at the end of the nanogel flooding. For the unsuccessful one, we find that some bigger droplets cannot be displaced and emulsified through the pore throat due to the capillary pressure and the nanogels are found adsorbed mostly on the droplet front meniscii. Potential mechanisms for in situ emulsification by nanogels are proposed and discussed. Under static global mode, we segment the images of remaining oil droplets before and after nanogel flooding, and their sphericity and diameter changes are compared and analyzed under different flow rates. The oil recovery for each experiment is enhanced by nanogel flooding, demonstrating the feasibility of using the nanogel as a potential EOR agent. However, the in situ emulsion by nanogels for EOR still needs further research using the 3D dual-porosity micromodels. The wettability effect on nanogel in situ emulsification could be investigated by altering the glass beads originally to be hydrophobic instead of hydrophilic. Besides, the nanogel concentration and surface charges could also be studied for better understanding its effect on the in situ emulsion generation and transportation under different conditions.

#### ASSOCIATED CONTENT

#### Supporting Information

The Supporting Information is available free of charge at https://pubs.acs.org/doi/10.1021/acs.langmuir.1c02029.

Interfacial tension activity between 0.1% nanogel suspension and immersion oil, nanogel (500 ppm) average size at different swelling times under 65 °C, nanogel (500 ppm) average size at different temperatures within 7 days, and nanogel (500 ppm)  $\zeta$  potential at different temperatures within 7 days (PDF)

Nanogel flooding after water flooding at 20 mL/h (MOV)

Water flooding (MOV)

#### AUTHOR INFORMATION

#### **Corresponding Authors**

Mingzhen Wei – Department of Geosciences and Geological and Petroleum Engineering, Missouri University of Science and Technology, Rolla 65409 Missouri, United States; Email: weim@mst.edu Wen Deng — School of Civil Engineering, Southeast University, Nanjing 211189 Jiangsu, China; ⊚ orcid.org/0000-0002-9544-8574; Email: wendeng@seu.edu.cn

#### **Authors**

Yandong Zhang — Department of Geosciences and Geological and Petroleum Engineering, Missouri University of Science and Technology, Rolla 65409 Missouri, United States

Jiaming Geng — Department of Geosciences and Geological and Petroleum Engineering, Missouri University of Science and Technology, Rolla 65409 Missouri, United States;
orcid.org/0000-0002-2889-2667

Junchen Liu – Department of Geosciences and Geological and Petroleum Engineering, Missouri University of Science and Technology, Rolla 65409 Missouri, United States

Baojun Bai – Department of Geosciences and Geological and Petroleum Engineering, Missouri University of Science and Technology, Rolla 6S409 Missouri, United States

Xiaoming He — Department of Mathematics and Statistics, Missouri University of Science and Technology, Rolla 65409 Missouri. United States

Complete contact information is available at: https://pubs.acs.org/10.1021/acs.langmuir.1c02029

#### Notes

The authors declare no competing financial interest.

#### ACKNOWLEDGMENTS

This research was supported by National Science Foundation grants 1722647. This research was also supported by the Fundamental Research Funds for the Central Universities (no. 3205002108C3).

#### REFERENCES

- (1) Pan, X.; Wang, L.; Dai, J.; Zhang, Q.; Peng, T.; Chen, W. Analysis of China's oil and gas consumption under different scenarios toward 2050: An integrated modeling. *Energy* **2020**, *195*, No. 116991.
- (2) Ramasamy, J.; Amanullah, M. Nanocellulose for oil and gas field drilling and cementing applications. *J. Pet. Sci. Eng.* **2020**, *184*, No. 106292.
- (3) ShamsiJazeyi, H.; Miller, C. A.; Wong, M. S.; Tour, J. M.; Verduzco, R. Polymer-coated nanoparticles for enhanced oil recovery. *J. Appl. Polym. Sci.* **2014**, *131*, No. 40576.
- (4) Green, D. W.; Willhite, G. P. In *Enhanced Oil Recovery*; Henry, L., Ed.; Doherty Memorial Fund of AIME, Society of Petroleum Engineers, 1998; Vol. 6.
- (5) Thomas, S. Enhanced oil recovery-an overview. Oil Gas Sci. Technol. Rev. IFP **2008**, 63, 9–19.
- (6) Ganesh, V. K. Nanotechnology in civil engineering. Eur. Sci. J. 2012, 8, 96–109.
- (7) Kubik, T.; Bogunia-Kubik, K.; Sugisaka, M. Nanotechnology on duty in medical applications. *Curr. Pharm. Biotechnol.* **2005**, *6*, 17–33.
- (8) Soppimath, K. S.; Aminabhavi, T. M.; Kulkarni, A. R.; Rudzinski, W. E. Biodegradable polymeric nanoparticles as drug delivery devices. *J. Controlled Release* **2001**, *70*, 1–20.
- (9) Kumari, A.; Yadav, S. K.; Yadav, S. C. Biodegradable polymeric nanoparticles based drug delivery systems. *Colloids Surf.*, B **2010**, 75, 1–18.
- (10) Liong, M.; Lu, J.; Kovochich, M.; Xia, T.; Ruehm, S. G.; Nel, A. E.; Tamanoi, F.; Zink, J. I. Multifunctional inorganic nanoparticles for imaging, targeting, and drug delivery. *ACS Nano* **2008**, *2*, 889–896.
- (11) Duncan, T. V. Applications of nanotechnology in food packaging and food safety: barrier materials, antimicrobials and sensors. *J. Colloid Interface Sci.* **2011**, 363, 1–24.

- (12) Saunders, B. R.; Turner, M. L. Nanoparticle-polymer photovoltaic cells. *Adv. Colloid Interface Sci.* **2008**, *138*, 1–23.
- (13) Rahmani, A. R.; Bryant, S.; Huh, C.; Athey, A.; Ahmadian, M.; Chen, J.; Wilt, M. Crosswell magnetic sensing of superparamagnetic nanoparticles for subsurface applications. *SPE J.* **2015**, *20*, 1067–1082.
- (14) Turkenburg, D.; Chin, P.; Fischer, H. In *Use of Modified Nanoparticles in Oil and Gas Reservoir Management*, SPE International Oilfield Nanotechnology Conference and Exhibition; Society of Petroleum Engineers, 2012.
- (15) Hoelscher, K. P.; De Stefano, G.; Riley, M.; Young, S. In *Application of Nanotechnology in Drilling Fluids*, SPE international oilfield nanotechnology conference and exhibition; Society of Petroleum Engineers: 2012.
- (16) Zhang, J.; Li, L.; Wang, S.; Wang, J.; Yang, H.; Zhao, Z.; Zhu, J.; Zhang, Z. In Novel Micro and Nano Particle-Based Drilling Fluids Pioneering Approach to Overcome the Borehole Instability Problem in Shale Formations, SPE Asia Pacific Unconventional Resources Conference and Exhibition; Society of Petroleum Engineers, 2015.
- (17) Mohammadizadeh, M.; Pourabbas, B.; Mahmoodian, M.; Foroutani, K.; Fallahian, M. Facile and rapid production of conductive flexible films by deposition of polythiophene nanoparticles on transparent poly (ethyleneterephthalate): Electrical and morphological properties. *Mater. Sci. Semicond. Process.* **2014**, *20*, 74–83.
- (18) Bennetzen, M. V.; Mogensen, K. In Novel Applications of Nanoparticles for Future Enhanced Oil Recovery, International Petroleum Technology Conference, Kuala Lumpur, Malaysia, December 2014.
- (19) Hashemi, R.; Nassar, N. N.; Almao, P. P. Nanoparticle technology for heavy oil in-situ upgrading and recovery enhancement: Opportunities and challenges. *Appl. Energy* **2014**, *133*, 374–387.
- (20) Alomair, O. A.; Matar, K. M.; Alsaeed, Y. H. Experimental study of enhanced-heavy-oil recovery in Berea sandstone cores by use of nanofluids applications. *SPE Reservoir Eval. Eng.* **2015**, *18*, 387–399.
- (21) Cheraghian, G.; Hendraningrat, L. A review on applications of nanotechnology in the enhanced oil recovery part A: effects of nanoparticles on interfacial tension. *Int. Nano Letters* **2016**, *6*, 129–138.
- (22) Hendraningrat, L.; Torsaeter, O. In Unlocking the Potential of Metal Oxides Nanoparticles to Enhance the Oil Recovery, Offshore Technology Conference-Asia, Kuala Lumpur, Malaysia, March 2014.
- (23) Bhattacharya, R.; Basu, J. Microscopic dynamics of nanoparticle monolayers at air—water interface. *J. Colloid Interface Sci.* **2013**, 396, 69–74.
- (24) Du, K.; Glogowski, E.; Emrick, T.; Russell, T. P.; Dinsmore, A. D. Adsorption energy of nano-and microparticles at liquid—liquid interfaces. *Langmuir* **2010**, *26*, 12518—12522.
- (25) Tian, C.; Feng, J.; Cho, H. J.; Datta, S. S.; Prud'homme, R. K. Adsorption and denaturation of structured polymeric nanoparticles at an interface. *Nano Lett.* **2018**, *18*, 4854–4860.
- (26) Saigal, T.; Yoshikawa, A.; Kloss, D.; Kato, M.; Golas, P. L.; Matyjaszewski, K.; Tilton, R. D. Stable emulsions with thermally responsive microstructure and rheology using poly (ethylene oxide) star polymers as emulsifiers. *J. Colloid Interface Sci.* **2013**, 394, 284–202
- (27) Li, X.; ShamsiJazeyi, H.; Pesek, S. L.; Agrawal, A.; Hammouda, B.; Verduzco, R. Thermoresponsive PNIPAAM bottlebrush polymers with tailored side-chain length and end-group structure. *Soft Matter* **2014**, *10*, 2008–2015.
- (28) Roustaei, A. An evaluation of spontaneous imbibition of water into oil-wet carbonate reservoir cores using nanofluid. *Petrophysics* **2014**, *55*, 31–37.
- (29) Cao, N.; Mohammed, M. A.; Babadagli, T. Wettability alteration of heavy-oil-bitumen-containing carbonates by use of solvents, high-pH solutions, and nano/ionic liquids. SPE Reservoir Evaluation & Engineering 2017, 20, 363–371.
- (30) Li, S.; Torsæter, Ö.; Lau, H. C.; Hadia, N. J.; Stubbs, L. P. The impact of nanoparticle adsorption on transport and wettability

- alteration in water-wet Berea sandstone: an experimental study. Front. Phys. 2019, 7, No. 74.
- (31) Nikolov, A.; Wasan, D. Spreading of nanofluids on solids. *Nature* **2003**, 423, 156–159.
- (32) Nikolov, A.; Kondiparty, K.; Wasan, D. Nanoparticle self-structuring in a nanofluid film spreading on a solid surface. *Langmuir* **2010**, *26*, *7665*–*7670*.
- (33) Zhang, T.; Davidson, D.; Bryant, S. L.; Huh, C. In *Nanoparticle-Stabilized Emulsions for Applications in Enhanced Oil Recovery*, SPE improved oil recovery symposium; Society of Petroleum Engineers, 2010.
- (34) Son, H.; Kim, H.; Lee, G.; Kim, J.; Sung, W. Enhanced oil recovery using nanoparticle-stabilized oil/water emulsions. *Korean J. Chem. Eng.* **2014**, *31*, 338–342.
- (35) Shen, X.; Ye, L. Interfacial molecular imprinting in nanoparticle-stabilized emulsions. *Macromolecules* **2011**, *44*, 5631–5637.
- (36) Kanj, M. Y.; Rashid, M.; Giannelis, E. *Industry First Field Trial of Reservoir Nanoagents*, SPE Middle East Oil and Gas Show and Conference; Society of Petroleum Engineers, 2011.
- (37) Agista, M. N.; Guo, K.; Yu, Z. A state-of-the-art review of nanoparticles application in petroleum with a focus on enhanced oil recovery. *Appl. Sci.* **2018**, *8*, 871.
- (38) Ding, H.; Zhang, N.; Zhang, Y.; Wei, M.; Bai, B. Experimental data analysis of nanoparticles for enhanced oil recovery. *Ind. Eng. Chem. Res.* **2019**, *58*, 12438–12450.
- (39) Hendraningrat, L.; Li, S.; Torsæter, O. A coreflood investigation of nanofluid enhanced oil recovery. *J. Pet. Sci. Eng.* **2013**, *111*, 128–138.
- (40) Kim, I.; Worthen, A. J.; Lotfollahi, M.; Johnston, K. P.; DiCarlo, D. A.; Huh, C. Nanoparticle-Stabilized Emulsions for Improved Mobility Control for Adverse-Mobility Waterflooding, IOR 2017-19th European Symposium on Improved Oil Recovery, IOR 2017-19th European Symposium on Improved Oil Recovery; European Association of Geoscientists & Engineers, 2017; pp 1–13.
- (41) Tian, S.; Gao, W.; Liu, Y.; Kang, W.; Yang, H. Effects of surface modification Nano-SiO2 and its combination with surfactant on interfacial tension and emulsion stability. *Colloids Surf., A* **2020**, 595, No. 124682.
- (42) Saha, R.; Uppaluri, R. V.; Tiwari, P. Silica nanoparticle assisted polymer flooding of heavy crude oil: emulsification, rheology, and wettability alteration characteristics. *Ind. Eng. Chem. Res.* **2018**, *57*, 6364–6376.
- (43) Zhou, Y.; Wu, X.; Zhong, X.; Sun, W.; Pu, H.; Zhao, J. X. Surfactant-Augmented functional silica nanoparticle based nanofluid for enhanced oil recovery at high temperature and salinity. *ACS Appl. Mater. Interfaces* **2019**, *11*, 45763–45775.
- (44) Zhou, Y.; Wu, X.; Zhong, X.; Reagen, S.; Zhang, S.; Sun, W.; Pu, H.; Zhao, J. X. Polymer nanoparticles based nano-fluid for enhanced oil recovery at harsh formation conditions. *Fuel* **2020**, 267, No. 117251.
- (45) Gbadamosi, A. O.; Junin, R.; Manan, M. A.; Yekeen, N.; Agi, A.; Oseh, J. O. Recent advances and prospects in polymeric nanofluids application for enhanced oil recovery. *J. Ind. Eng. Chem.* **2018**, *66*, 1–10.
- (46) Geng, J.; Pu, J.; Zhao, Y.; Lin, B.; Bai, B.; Thomas, S. P. pH-Responsive crude oil-in-water Pickering emulsion stabilized by polyacrylamide nanogels. *Fuel* **2019**, 258, No. 116159.
- (47) Geng, J.; Pu, J.; Wang, L.; Bai, B. Surface charge effect of nanogel on emulsification of oil in water for fossil energy recovery. *Fuel* **2018**, 223, 140–148.
- (48) Destribats, M.; Lapeyre, V.; Wolfs, M.; Sellier, E.; Leal-Calderon, F.; Ravaine, V.; Schmitt, V. Soft microgels as Pickering emulsion stabilisers: role of particle deformability. *Soft Matter* **2011**, *7*, 7689–7698.
- (49) Almahfood, M.; Bai, B. The synergistic effects of nanoparticle-surfactant nanofluids in EOR applications. *J. Pet. Sci. Eng.* **2018**, *171*, 196–210.

- (50) Geng, J.; Ding, H.; Han, P.; Wu, Y.; Bai, B. Transportation and potential enhanced oil recovery mechanisms of nanogels in sandstone. *Energy Fuels* **2018**, *32*, 8358–8365.
- (51) Qin, T.; Goual, L.; Piri, M.; Hu, Z.; Wen, D. Pore-scale dynamics of nanofluid-enhanced NAPL displacement in carbonate rock. *J. Contam. Hydrol.* **2020**, 230, No. 103598.
- (52) Li, S.; Hendraningrat, L.; Torsaeter, O. *Improved Oil Recovery by Hydrophilic Silica Nanoparticles Suspension: 2 Phase Flow Experimental Studies*, IPTC 2013: International Petroleum Technology Conference; European Association of Geoscientists & Engineers, 2013; cp-350-00212.
- (53) Conn, C. A.; Ma, K.; Hirasaki, G. J.; Biswal, S. L. Visualizing oil displacement with foam in a microfluidic device with permeability contrast. *Lab Chip* **2014**, *14*, 3968–3977.
- (54) Zhang, Y.; Zhou, C.; Qu, C.; Wei, M.; He, X.; Bai, B. Fabrication and verification of a glass-silicon-glass micro-/nano-fluidic model for investigating multi-phase flow in shale-like unconventional dual-porosity tight porous media. *Lab Chip* **2019**, 19, 4071–4082.
- (55) Nguyen, P.; Fadaei, H.; Sinton, D. Nanoparticle Stabilized CO2 in Water Foam for Mobility Control in Enhanced Oil Recovery Via Microfluidic Method, SPE Heavy Oil Conference-Canada; Society of Petroleum Engineers, 2014.
- (56) Cheraghian, G.; Kiani, S.; Nassar, N. N.; Alexander, S.; Barron, A. R. Silica nanoparticle enhancement in the efficiency of surfactant flooding of heavy oil in a glass micromodel. *Ind. Eng. Chem. Res.* **2017**, 56, 8528–8534.
- (57) Tajik, S.; Shahrabadi, A.; Rashidi, A.; Jalilian, M.; Yadegari, A. Application of functionalized silica-graphene nanohybrid for the enhanced oil recovery performance. *Colloids Surf., A* **2018**, *556*, 253–265.
- (58) Xu, K.; Zhu, P.; Huh, C.; Balhoff, M. T. Microfluidic investigation of nanoparticles' role in mobilizing trapped oil droplets in porous media. *Langmuir* **2015**, *31*, 13673–13679.
- (\$9) Xu, K.; Liang, T.; Zhu, P.; Qi, P.; Lu, J.; Huh, C.; Balhoff, M. A 2.5-D glass micromodel for investigation of multi-phase flow in porous media. *Lab Chip* **2017**, *17*, 640–646.
- (60) Xu, K.; Agrawal, D.; Darugar, Q. Hydrophilic nanoparticle-based enhanced oil recovery: microfluidic investigations on mechanisms. *Energy Fuels* **2018**, *32*, 11243–11252.
- (61) Yang, Y.; Cheng, T.; Wu, H.; You, Z.; Shang, D.; Hou, J. Enhanced Oil Recovery Using Oleic Acid-Modified Titania Nanofluids: Underlying Mechanisms and Oil-Displacement Performance. *Energy Fuels* **2020**, *34*, 5813–5822.
- (62) Krummel, A. T.; Datta, S. S.; Münster, S.; Weitz, D. A. Visualizing multiphase flow and trapped fluid configurations in a model three-dimensional porous medium. *AIChE J.* **2013**, *59*, 1022–1029.
- (63) Datta, S. S.; Dupin, J.-B.; Weitz, D. A. Fluid breakup during simultaneous two-phase flow through a three-dimensional porous medium. *Phys. Fluids* **2014**, *26*, No. 062004.
- (64) do Nascimento, D. F.; Junior, J. R. V.; Paciornik, S.; Carvalho, M. S. Pore scale visualization of drainage in 3D porous media by confocal microscopy. *Sci. Rep.* **2019**, *9*, No. 12333.
- (65) Zhang, L.; Abbaspourrad, A.; Parsa, S.; Tang, J.; Cassiola, F. M.; Zhang, M.; Tian, S.; Dai, C.; Xiao, L.; Weitz, D. A. Core-shell Nanohydrogels with Programmable Swelling for Conformance Control in Porous Media. ACS Appl. Mater. Interfaces 2020, 12, 34217–34225.
- (66) Bizmark, N.; Ioannidis, M. A.; Henneke, D. E. Irreversible adsorption-driven assembly of nanoparticles at fluid interfaces revealed by a dynamic surface tension probe. *Langmuir* **2014**, *30*, 710–717.
- (67) Behrens, S. H.; Grier, D. G. The charge of glass and silica surfaces. *J. Chem. Phys.* **2001**, *115*, 6716–6721.
- (68) Johnson, C. A.; Lenhoff, A. M. Adsorption of charged latex particles on mica studied by atomic force microscopy. *J. Colloid Interface Sci.* **1996**, *179*, 587–599.

- (69) Thompson, K. E.; Willson, C. S.; White, C. D.; Nyman, S.; Bhattacharya, J. P.; Reed, A. H. Application of a new grain-based reconstruction algorithm to microtomography images for quantitative characterization and flow modeling. SPE J. 2008, 13, 164–176.
- (70) Metin, C.; Bonnecaze, R.; Nguyen, Q. The viscosity of silica nanoparticle dispersions in permeable media. *SPE Reservoir Eval. Eng.* **2013**, *16*, 327–332.
- (71) Hou, J.; Qiu, M.; He, X.; Guo, C.; Wei, M.; Bai, B. A dual-porosity-Stokes model and finite element method for coupling dual-porosity flow and free flow. *SIAM J. Sci. Comput.* **2016**, *38*, B710–B739
- (72) Deng, W.; Balhoff, M.; Cardenas, M. B. Influence of dynamic factors on nonwetting fluid snap-off in pores. *Water Resour. Res.* **2015**, *51*, 9182–9189.
- (73) Deng, W.; Cardenas, M. B.; Bennett, P. C. Extended Roof snapoff for a continuous nonwetting fluid and an example case for supercritical CO<sub>2</sub>. Adv. Water Resour. **2014**, *64*, 34–46.
- (74) Kwok, M.-h.; Ngai, T. A confocal microscopy study of micronsized poly (N-isopropylacrylamide) microgel particles at the oil—water interface and anisotopic flattening of highly swollen microgel. *J. Colloid Interface Sci.* **2016**, *461*, 409–418.
- (75) Soo, H.; Radke, C. Velocity effects in emulsion flow through porous media. *I. Colloid Interface Sci.* 1984, 102, 462–476.
- (76) Fu, Y.; Zhao, S.; Bai, L.; Jin, Y.; Cheng, Y. Numerical study of double emulsion formation in microchannels by a ternary Lattice Boltzmann method. *Chem. Eng. Sci.* **2016**, *146*, 126–134.
- (77) Rezaei, N.; Firoozabadi, A. Macro-and Microscale Water-flooding Performances of Crudes which form w/o Emulsions upon Mixing with Brines. *Energy Fuels* **2014**, *28*, 2092–2103.
- (78) Liu, M.; Liu, Y.; Li, J.; Chen, S.; Li, J.; Su, L.; bo Qi, X.; Li, B.; Zhang, Z. Improvement of sphericity of thick-walled polystyrene shell. *Colloids Surf., A* **2015**, 484, 463–470.
- (79) Luo, D.; Wang, F.; Zhu, J.; Cao, F.; Liu, Y.; Li, X.; Willson, R. C.; Yang, Z.; Chu, C.-W.; Ren, Z. Nanofluid of graphene-based amphiphilic Janus nanosheets for tertiary or enhanced oil recovery: High performance at low concentration. *Proc. Natl. Acad. Sci. U.S.A.* **2016**, *113*, 7711–7716.
- (80) Zhou, Y.; Wang, D.; Wang, Z.; Cao, R. The formation and viscoelasticity of pore-throat scale emulsion in porous media. *Pet. Explor. Dev.* **2017**, *44*, 111–118.
- (81) Datta, S. S.; Chiang, H.; Ramakrishnan, T.; Weitz, D. A. Spatial fluctuations of fluid velocities in flow through a three-dimensional porous medium. *Phys. Rev. Lett.* **2013**, *111*, No. 064501.